MPC-based Torque Distribution for Planar Motion of Four-wheel Independently Driven Electric Vehicles: Considering Motor Models and Iron Losses

Yiyan Su, Deliang Liang, *Senior Member, IEEE*, and Peng, Kou, *Senior Member*, *IEEE*

Abstract—The most critical obstacle for four-wheel independently driven electric vehicles (4WID-EVs) is the driving range. Being the actuators of 4WID-EVs, motors account for its major power consumption. In this sense, by properly distributing torques to minimize the power consumption, the driving range of 4WID-EV can be effectively improved. This paper proposes a model predictive control (MPC)-based torque distribution scheme, which minimizes the power consumption of 4WID-EVs while guaranteeing its tracking performance of planar motions. By incorporating the motor model considering iron losses, the optimal torque distribution can be achieved without an additional torque controller. Also, for this reason, the proposed control scheme is computationally efficient, since the power consumption term to be optimized, which is expressed as the product of the motor voltages and currents, is much simpler than that derived from the efficiency map. With reasonable simplification and linearization, the MPC problem is converted to a quadratic programming problem, which can be solved efficiently. The simulation results in MATLAB and CarSim co-simulation environments demonstrate that the proposed scheme effectively reduces power consumption with guaranteed tracking performance.

Index Terms—four-wheel independently driven electric vehicles, Model predictive control, Motor models, Iron losses.

I. Introduction

ELECTRIC vehicles (EVs) have attracted increasing attention due to the advantages of lower emission and higher energy efficiency. Among various types of EVs, the four-wheel independently driven (4WID) EVs offer greater control flexibility due to four independently controllable motors, thus having more potential in improving tracking performance and reducing power consumption [1]-[3]. Moreover, because of the unique powertrain configuration, the reducer and transmission are not equipped in 4WID-EVs. For this reason, the complexity of the powertrain can be greatly

reduced, and more space can be provided for other modules especially large energy storage systems [4].

The driving range is a great obstacle that limits the rapid development of EVs [5]. Being the actuators of EVs, motors account for the major power consumption and realize the exchange of electric and mechanical power. Especially for 4WID-EVs, this influence of motor power consumption on driving range becomes more significant, since there is no additional power consumption caused by transmissions and reducers. However, considering its unique powertrain configuration and control flexibility, 4WID-EVs can realize more complicated and flexible torque distributions by independently controlling each motor, thus giving the potential to reduce total power consumption while guaranteeing tracking performance [6]-[8]. In this sense, computing the optimal energy-efficient torque distribution is an effective and practical approach to increase the driving range for 4WID-EVs.

Inspired by this, many publications have already proposed innovative control strategies for planar motion control of 4WID-EVs. In [5], the optimal torque distribution was computed considering a practicable motor energy efficiency model. In [9], an optimal torque distribution was achieved to improve the traction efficiency and braking energy recovery using an offline genetic algorithm. In [10], a Karush-Kuhn-Tucker-based algorithm was presented to quickly achieve an energy-efficient control allocation taking both the actuators' efficiencies and the operation modes into account. In [11], the velocity and torque distribution were optimized by a nonlinear model predictive controller according to the preceding vehicle motions. In [12], the torque distribution was optimized based on the experimental characterizations of a prototyping pure electric vehicle. In [13], the controller used a nonlinear model predictive controller to solve the tracking problem based on the nonlinear vehicle dynamics model. In [14], PI controller and adaptive sliding mode controller were respectively implemented to control the longitudinal and yaw motion. The control distribution computed by quadratic programming coordinates the four motors to minimize tracking errors and utilization rate of tire. In [15], the controller distributed the virtual control signals to four motors with an adaptive convergence to the optimal operating points.

For all above control schemes, the motor model was not considered. As a result, the optimized control actions in these schemes were virtual torque control signals and, hence, additional torque controllers were required to implement these torque control signals. Due to the dynamic limits of the torque controller, the actual torque distribution may be different from the optimized solution, and the performance of tracking and energy saving will deteriorate if the parameters of the corresponding torque control algorithm are not well optimized. Meanwhile, in the existing studies, the control-oriented vehicle dynamics model was usually nonlinear, so most of the existing studies solved the control problem using complicated nonlinear optimization algorithms, e.g., genetic algorithm and nonlinear model predictive control, which are, in general, computationally heavy and impractical for real-time applications. The exception is [15], which directly incorporated the motor efficiency map into the computation of torque distribution by piecewise linearization. However, this also leads to high computational cost due to the constructed nonlinear power consumption term to be optimized. Moreover, in this paper, the torque constraint was regarded as constant, which is unreasonable since the torque limit varies with the operating state of motors under the voltage and current limits.

After reviewing these previous works, we find that a feasible way to overcome the aforementioned shortcomings is to explicitly consider motor models and iron losses in control schemes design. The reason for this is three-fold. First, the motor model contains a latent relationship between the torque and the motor voltages. Therefore, after considering motor models in the control scheme design, we can directly compute the motor voltages corresponding to the desired torque. The desired torque can be realized by imposing the corresponding voltage signals to motors' terminals. By this means, an additional torque controller can be omitted, and the number of adjustable parameters is reduced. Second, by considering iron losses in motor models, the motor model does not only reflect the dynamic characteristic, but also the power consumption of motors. The power consumption can be computed by the product of the motor voltage and current, so the efficiency map can be omitted. In this way, the power consumption term to be optimized is simpler than that of the method using the efficiency map, and hence, the computational cost is lower. Third, once the motor voltage and current constraints are determined, the torque constraint varies with the electrical angular velocity. By properly setting the motor voltage and current constraints, the motor torque can be implicitly constrained, thereby reducing the number of constraints in the optimization problem. According to the above analysis, after considering motor models and iron losses, the planar motion control of 4WID-EV is essentially optimizing the torque distribution, which minimizes the power consumption and tracking errors, subject to the corresponding voltage and current constraints. This is, in fact, a constrained optimal control problem. The model predictive control (MPC) is an excellent approach to solve such a control problem.

Inspired by the above analysis, this paper proposes an MPC-based torque distribution scheme for planar motion control of 4WID-EVs. The control objectives are twofold, i.e., to minimize the power consumption and guarantee the tracking performance. To achieve these objectives, the vehicle dynamics model and motor model with iron losses are established. Based on the motor model considering iron losses, an MPC controller is developed to optimize the control actions for four motors. The computed control actions are motor voltage signals, which correspond to the optimal torque distribution. With this scheme, the optimal torque distribution can be directly achieved without an additional torque controller. A salient feature of this scheme is that, by incorporating the linearized motor models considering iron losses, the MPC problem can be formulated as a standard quadratic programming problem, which can be solved efficiently.

The remainder of this paper is organized as follows. Section II presents the vehicle dynamics model and the improved motor model considering iron losses. The MPC-based scheme is developed in Section III. In Section IV, simulation results are illustrated to verify the effectiveness of the proposed scheme compared with the conventional torque distribution schemes. Finally, conclusions are presented in Section V.

II. SYSTEM MODELING

In order to design the MPC-based torque distribution scheme for planar motions of 4WID-EVs, the dynamics model of 4WID-EV and the motor model considering iron losses are required. The detailed descriptions of these models are shown in this section.

A. 4WID-EV Dynamics Model

Planar motions are the most energy-consuming movements of vehicles, so this paper aims at planar motions of 4WID-EVs. The dynamic model considering only the planar motion under the front-wheel steering of 4WID-EVs is shown in Fig. 1.
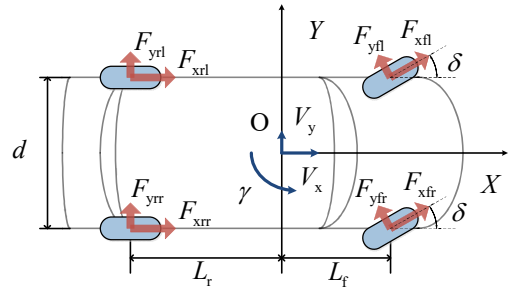

Fig. 1. The 4WID-EV dynamics model for planar motion.

Considering only the planar motion, the electric vehicle can be modeled as a rigid body with three degrees of freedom: v_x, v_y, and γ, which are the longitudinal velocity, lateral velocity, and yaw rate of the vehicle, respectively. Based on Fig. 1, the dynamic equations of the planar motion of 4WID-EVs can be written as

$$
\begin{aligned}
\dot{v}_x &= \frac{1}{m}[(F_{xfl}+F_{xfr})\cos\delta+F_{xrl}+F_{xrr}-(F_{yfl}+F_{yfr})\sin\delta]+v_y\gamma \\
\dot{v}_y &= \frac{1}{m}[(F_{yfl}+F_{yfr})\cos\delta+F_{yrl}+F_{yrr}+(F_{xfl}+F_{xfr})\sin\delta]-v_x\gamma \\
\dot{\gamma} &= \frac{1}{I_z}[L_f(F_{xfl}+F_{xfr})\sin\delta+L_f(F_{yfl}+F_{yfr})\cos\delta-L_r(F_{yrl}+F_{yrr}) \\
&\quad +\frac{d}{2}(F_{xfr}-F_{xfl})\cos\delta+\frac{d}{2}(F_{xrr}-F_{xrl})+\frac{d}{2}(F_{yfl}-F_{yfr})\sin\delta]
\end{aligned}
\tag{1}
$$

SU et al. : MPC-BASED TORQUE DISTRIBUTION FOR PLANAR MOTION OF FOUR-WHEEL INDEPENDENTLY DRIVEN ELECTRIC VEHICLES: CONSIDERING MOTOR MODELS AND IRON LOSSES

47

In (1), m is the vehicle mass, I_z is the vehicle yaw moment of inertia. F_{xj} and F_{yj} respectively represent the tire longitudinal and lateral forces, and the subscript $j \in \{fl,fr,rl,rr\}$ represents different wheels. The wheel steering angles of the front left and right wheels are assumed to be the same, which are marked as δ. L_f and L_r are the front and rear semi wheelbase. d is the width of the vehicle.

In daily driving scenarios, planar motions with small wheel steering angles and medium speed are common. For this driving situation, the power consumption optimization and driving range expansion are significant control objectives. Considering these two facts, planar motions with small wheel steering angles and medium speed are studied in this paper, and the longitudinal and yaw motions of vehicles are controlled. This way, the dynamic equations (1) can be simplified with the assumptions $\cos\delta \approx 1$ and $\sin\delta \approx 0$ as

$$\dot{v}_x = \frac{1}{m}[(F_{xfl}+F_{xfr})+F_{xrl}+F_{xrr}]+v_y\gamma$$
$$\dot{\gamma} = \frac{1}{I_z}[L_f(F_{yfl}+F_{yfr})-L_r(F_{yrl}+F_{yrr})+\frac{d}{2}(F_{xfr}-F_{xfl})+\frac{d}{2}(F_{xrr}-F_{xrl})].$$

(2)

4WID-EVs is an over-actuated system, in which the number of motors is larger than the degrees of freedom [16]-[18]. For a general over-actuated system, its dynamic model can be described as

$$\dot{\mathbf{x}} = f(\mathbf{x}) + g(\mathbf{x})\mathbf{v}_d, \quad \mathbf{v}_d = \mathbf{Bu}, \quad \mathbf{y} = h(\mathbf{x})$$ (3)

In (3), $\mathbf{x}$ is the system state vector, $\mathbf{v}_d$ is the virtual control vector, $\mathbf{B}$ is the control effectiveness matrix, $\mathbf{u}$ is the control input vector, and $\mathbf{y}$ is the system output vector. As for the 4WID-EV investigated in this paper, model (3) can be rewritten as

$$\begin{bmatrix} \dot{v}_x \\ \dot{\gamma} \end{bmatrix} = \begin{bmatrix} v_y\gamma \\ \frac{L_f}{I_z}(F_{yfl}+F_{yfr})-\frac{L_r}{I_z}(F_{yrl}+F_{yrr}) \end{bmatrix} + \begin{bmatrix} \frac{1}{m} & 0 \\ 0 & \frac{1}{I_z} \end{bmatrix}\begin{bmatrix} \sum F_{xj} \\ M_z \end{bmatrix}$$

$$\begin{bmatrix} \sum F_{xj} \\ M_z \end{bmatrix} = \begin{bmatrix} 1 & 1 & 1 & 1 \\ -\frac{d}{2} & \frac{d}{2} & -\frac{d}{2} & \frac{d}{2} \end{bmatrix}\begin{bmatrix} F_{xfl} \\ F_{xfr} \\ F_{xrl} \\ F_{xrr} \end{bmatrix}.$$

(4)

The motion of the 4WID-EV is directly determined by the comprehensive effect of the tire forces. The longitudinal forces F_{xj} and lateral forces F_{yj} are primarily determined by the vertical load, the wheel side slip angle, and the longitudinal slip ratio. The relationships are nonlinear and complex. In order to simplify the analysis, the longitudinal forces are obtained from the rotational dynamics of each motor and wheel pair without relying on the tire model. Interested readers are referred to [13] for more details about the nonlinear tire model.

The rotational dynamics equations of the motor and wheel pairs are expressed as

$$[\dot{\omega}_{rfl} \; \dot{\omega}_{rfr} \; \dot{\omega}_{rrl} \; \dot{\omega}_{rrr}]^T = \frac{1}{J}[T_{fl} \; T_{fr} \; T_{rl} \; T_{rr}]^T$$
$$-\frac{R}{J}[F_{xfl} \; F_{xfr} \; F_{xrl} \; F_{xrr}]^T$$

(5)

where ω_{rj}, T_j, R, and J respectively represent the mechanical

angular velocity, motor output torques, the tire effective radius, and the rotational moment of inertia. According to (5), the longitudinal forces of tires can be obtained by assuming that the mechanical angular velocity remains constant in each control circle. This assumption is reasonable when the sample time is small enough. By doing so, the rotational dynamics can be described as

$$[F_{xfl} \; F_{xfr} \; F_{xrl} \; F_{xrr}]^T = \frac{1}{R}[T_{fl} \; T_{fr} \; T_{rl} \; T_{rr}]^T$$ (6)

Combining (4) and (6), the control-oriented dynamics model of 4WID-EVs is finally expressed as

$$\begin{bmatrix} \dot{v}_x \\ \dot{\gamma} \end{bmatrix} = \begin{bmatrix} v_y\gamma \\ \frac{L_f}{I_z}(F_{yfl}+F_{yfr})-\frac{L_f}{I_z}(F_{yrl}+F_{yrr}) \end{bmatrix} + \begin{bmatrix} \frac{1}{m} & 0 \\ 0 & \frac{1}{I_z} \end{bmatrix}\begin{bmatrix} \sum F_{xj} \\ M_z \end{bmatrix}$$

$$\begin{bmatrix} \sum F_{xj} \\ M_z \end{bmatrix} = \begin{bmatrix} \frac{1}{R} & \frac{1}{R} & \frac{1}{R} & \frac{1}{R} \\ -\frac{d}{2R} & \frac{d}{2R} & -\frac{d}{2R} & \frac{d}{2R} \end{bmatrix}\begin{bmatrix} T_{fl} \\ T_{fr} \\ T_{rl} \\ T_{rr} \end{bmatrix}.$$

(7)

B. In-wheel Motor Models Considering Iron Losses

Permanent magnet synchronous motors (PMSMs) are widely used in 4WID-EVs due to the high efficiency, high power density, and superior dynamic performance [19]-[21]. This paper also selects PMSM as the research object. Ignoring the friction loss and stray loss which are usually tiny, the power loss of motors can be generally classified into copper losses and iron losses. According to previous researches on energy efficiency and power loss of PMSMs, iron losses have a significant impact on the efficiency and it will lead to a higher deviation between the efficiency of the motor model and that of the actual PMSM if modeling the motor without considering iron losses [22][23]. To address this, an improved motor model considering iron losses is required.

According to [24]-[26], the improved rotor-flux-oriented equivalent circuits of a PMSM considering iron losses are shown in Fig. 2.
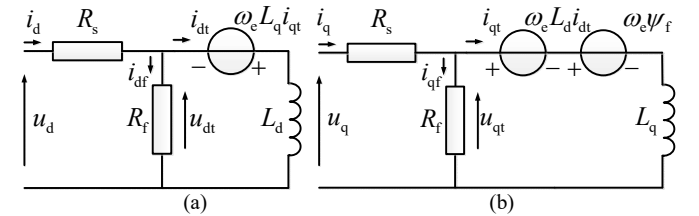

Fig. 2. Equivalent circuits of the PMSM considering iron losses. (a) D-axis equivalent circuits. (b) Q-axis equivalent circuits.

In Fig. 2, i_d and i_q are d-, q-axis current components. u_d and u_q are the d-, q-axis voltage components. i_{df} and i_{qf} are d-, q-axis iron loss current components. i_{dt} and i_{qt} are d-, q-axis magnetizing current components. R_s is the stator resistance. R_f is the iron loss resistance. ω_e is the electrical angular velocity. L_d and L_q are the d-, q-axis inductance components. Ψ_f is the permanent magnet flux linkage.

In order to simplify the analysis and calculation, the iron loss current is computed according to the steady state of the motor with the assumption that PMSMs have constant iron losses in both transient and steady state [27]. In this case, the d-q axis

current equations can be written as

$$i_{\mathrm{df}} = -\frac{\omega_e L_q i_{qt}}{R_f}, \quad i_{qf} = \frac{\omega_e(L_d i_{dt} + \psi_f)}{R_f}$$

$$i_{dt} = \frac{1}{1 + \dfrac{\omega_e^2 L_d L_q}{R_f^2}}\left(i_d + \frac{\omega_e L_q}{R_f}i_q - \frac{\omega_e^2 L_q \psi_f}{R_f^2}\right),$$

$$i_{qt} = \frac{1}{1 + \dfrac{\omega_e^2 L_d L_q}{R_f^2}}\left(i_q - \frac{\omega_e L_d}{R_f}i_d - \frac{\omega_e \psi_f}{R_f}\right) \tag{8}$$

Similarly, the *d-q* axis voltage equations are expressed as

$$u_d = R_s i_d +$$
$$\frac{1}{1 + \dfrac{\omega_e^2 L_d L_q}{R_f^2}}\left(\frac{\omega_e^2 L_d L_q}{R_f}i_d + L_d\frac{di_d}{dt} - \omega_e L_q i_q + \frac{\omega_e L_d L_q}{R_f}\frac{di_q}{dt} + \frac{\omega_e^2 L_q}{R_f}\psi_f\right)$$

$$u_q = R_s i_q + \omega_e \psi_f +$$
$$\frac{1}{1 + \dfrac{\omega_e^2 L_d L_q}{R_f^2}}\left(\frac{\omega_e^2 L_d L_q}{R_f}i_q + L_q\frac{di_q}{dt} + \omega_e L_d i_d - \frac{\omega_e L_d L_q}{R_f}\frac{di_d}{dt} - \frac{\omega_e^3 L_d L_q}{R_f^2}\psi_f\right). \tag{9}$$

For the surface permanent magnet synchronous motor (SPMSM) used in this paper, the motor model is derived from (8) and (9) as follows:

$$\begin{bmatrix} \dot{i}_d \\ \dot{i}_q \end{bmatrix} = \begin{bmatrix} -\dfrac{R_s}{L_s} & \left(\dfrac{R_s}{R_f}+1\right)\omega_e \\ -\left(\dfrac{R_s}{R_f}+1\right)\omega_e & -\dfrac{R_s}{L_s} \end{bmatrix}\begin{bmatrix} i_d \\ i_q \end{bmatrix} +$$

$$\begin{bmatrix} \dfrac{1}{L_s} & -\dfrac{\omega_e}{R_f} \\ \dfrac{\omega_e}{R_f} & \dfrac{1}{L_s} \end{bmatrix}\begin{bmatrix} u_d \\ u_q \end{bmatrix} + \begin{bmatrix} 0 \\ -\dfrac{\omega_e \psi_f}{L_s} \end{bmatrix} \tag{10}$$

$$T_e = \frac{1}{1 + \dfrac{\omega_e^2 L_s^2}{R_f^2}}\left(p_n\psi_f i_q - \frac{p_n\psi_f \omega_e L_s}{R_f}i_d - \frac{p_n\psi_f^2 \omega_e}{R_f}\right)$$

In general, the parameters of the SPMSM satisfy

$$\frac{\omega_e^2 L_s^2}{R_f^2} \ll 1 , \quad \frac{R_s}{R_f} \ll 1 \tag{11}$$

so, (10) can be simplified as

$$\begin{bmatrix} \dot{i}_d \\ \dot{i}_q \end{bmatrix} = \begin{bmatrix} -\dfrac{R_s}{L_s} & \omega_e \\ -\omega_e & -\dfrac{R_s}{L_s} \end{bmatrix}\begin{bmatrix} i_d \\ i_q \end{bmatrix} + \begin{bmatrix} \dfrac{1}{L_s} & -\dfrac{\omega_e}{R_f} \\ \dfrac{\omega_e}{R_f} & \dfrac{1}{L_s} \end{bmatrix}\begin{bmatrix} u_d \\ u_q \end{bmatrix} + \begin{bmatrix} 0 \\ -\dfrac{\omega_e \psi_f}{L_s} \end{bmatrix} \tag{12}$$

$$T_e = p_n\psi_f i_q - \frac{p_n\psi_f \omega_e L_s}{R_f}i_d - \frac{p_n\psi_f^2 \omega_e}{R_f}.$$

This is the PMSM model in *d-q* axis considering iron losses, in which the iron loss is equivalent to the power lost on R_f.

III. PROBLEM FORMULATION AND CONTROLLER DESIGN

A. Control Problem Formulation

In the common driving scenarios with medium speed and small wheel steering angles, energy saving is an important requirement of the control scheme to improve the driving range.

The energy-saving performance determines the quality of the control scheme. Therefore, the most important control objective is to minimize the total power consumption during the whole driving cycle. Another fundamental control objective is to guarantee the tracking performance of the longitudinal velocity and yaw rate, thus making the vehicle follow the desired trajectory. Besides, to ensure the real-time property, the controller should be computationally light. The achievement of the above two control objectives strongly depends on the optimal distribution of torques among four motors. Therefore, an MPC-based torque distribution scheme is presented in this paper. The overall control scheme structure is shown in Fig. 3.
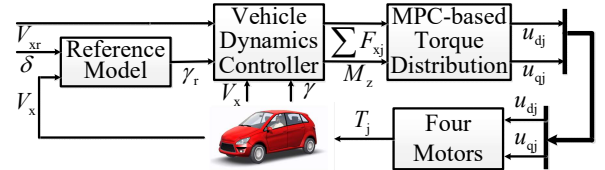

Fig. 3. The overall control scheme structure.

In the MPC-based scheme, the optimal energy-efficient torque distribution is computed. The computed control actions are voltages u_{dj} and u_{qj}. The desired total longitudinal forces $\sum F_{xj}$ and yaw moment M_z is computed by the vehicle dynamics controller. The expected longitudinal velocity and yaw rate are obtained from the reference model, which is designed in the framework of the linear two-degree-of-freedom model [28].

B. MPC-based Torque Distribution Scheme Design

In the MPC framework, an internal discrete-time prediction model must be specified to predict the future behavior of the variables to be controlled. For the motor model, the variables to be controlled are the *d-q* axis currents. In light of this, its prediction model should be derived based on the dynamics model of 4WID-EV (7) and the PMSM model (12). For the convenience of expression, we have modified the subscript j, using the subscript j ∈ {1,2,3,4} respectively represents the front left, front right, rear left, and rear right motors. From model (12), for each *j*-th motor, the dynamic model includes the nonlinear terms $\omega_{ej}i_{qj}$ and $\omega_{ej}i_{dj}$ needed to be linearized.

In order to linearize the model (12), the rotor mechanical angular velocity ω_{mj} is assumed to be constant for each control cycle. This is a valid approximation when the sample time is small enough. Consequently, the rotor electrical angular velocity ω_{ej} can also be assumed constant in each control cycle. With this assumption, the dynamics of i_{dj} and i_{qj} are decoupled from ω_{ej}. Using the exponential discretization, we can obtain a discrete-time state-space model of the *j*-th PMSM, as follows

$$\begin{bmatrix} i_{dj}(k+1) \\ i_{qj}(k+1) \end{bmatrix} = \mathbf{A}_j\begin{bmatrix} i_{dj}(k) \\ i_{qj}(k) \end{bmatrix} + \mathbf{B}_j\begin{bmatrix} u_{dj}(k) \\ u_{qj}(k) \end{bmatrix} + \begin{bmatrix} 0 \\ T_s \end{bmatrix}\left(-\frac{\omega_{ej}\psi_f}{L_s}\right)$$

$$\mathbf{T}_j(k) = \begin{bmatrix} -\dfrac{p_n\psi_f \omega_{ej}L_s}{R_{fj}} & p_n\psi_f \end{bmatrix}\begin{bmatrix} i_{dj}(k) \\ i_{qj}(k) \end{bmatrix} - \frac{p_n\psi_f^2 \omega_{ej}}{R_{fi}} \tag{13}$$

with

$$\mathbf{A}_j = \exp\left(\begin{bmatrix} -\dfrac{R_s}{L_s} & \omega_{ej} \\ -\omega_{ej} & -\dfrac{R_s}{L_s} \end{bmatrix}T_s\right), \quad \mathbf{B}_j = \begin{bmatrix} -\dfrac{R_s}{L_s} & \omega_{ej} \\ -\omega_{ej} & -\dfrac{R_s}{L_s} \end{bmatrix}^{-1}(\mathbf{A}_j - \mathbf{I})\begin{bmatrix} \dfrac{1}{L_s} & -\dfrac{\omega_{ej}}{R_{fj}} \\ \dfrac{\omega_{ej}}{R_{fj}} & \dfrac{1}{L_s} \end{bmatrix}$$

Here, T_s is the sampling period and k is the time step. This discrete-time model is used to predict the future behavior of the PMSM. Combining (7) and (13), the model used as the internal prediction model for the MPC-based scheme design can be expressed as

$$
\underbrace{\begin{bmatrix} i_{d1}(k+1) \\ i_{q1}(k+1) \\ i_{d2}(k+1) \\ i_{q2}(k+1) \\ i_{d3}(k+1) \\ i_{q3}(k+1) \\ i_{d4}(k+1) \\ i_{q4}(k+1) \end{bmatrix}}_{\mathbf{x}(k+1)} = \underbrace{\begin{bmatrix} \mathbf{A_1} & & & \\ & \mathbf{A_2} & & \\ & & \mathbf{A_3} & \\ & & & \mathbf{A_4} \end{bmatrix}}_{\mathbf{A}} \underbrace{\begin{bmatrix} i_{d1}(k) \\ i_{q1}(k) \\ i_{d2}(k) \\ i_{q2}(k) \\ i_{d3}(k) \\ i_{q3}(k) \\ i_{d4}(k) \\ i_{q4}(k) \end{bmatrix}}_{\mathbf{x}(k)}
$$

$$
+ \underbrace{\begin{bmatrix} \mathbf{B_1} & & & \\ & \mathbf{B_2} & & \\ & & \mathbf{B_3} & \\ & & & \mathbf{B_4} \end{bmatrix}}_{\mathbf{B}} \underbrace{\begin{bmatrix} u_{d1} \\ u_{q1} \\ u_{d2} \\ u_{q2} \\ u_{d3} \\ u_{q3} \\ u_{d4} \\ u_{q4} \end{bmatrix}}_{\mathbf{u}(k)} + \underbrace{\begin{bmatrix} 0 & 0 & 0 & 0 \\ T_s & 0 & 0 & 0 \\ 0 & 0 & 0 & 0 \\ 0 & T_s & 0 & 0 \\ 0 & 0 & 0 & 0 \\ 0 & 0 & T_s & 0 \\ 0 & 0 & 0 & 0 \\ 0 & 0 & 0 & T_s \end{bmatrix}}_{\mathbf{\acute{E}}} \underbrace{\begin{bmatrix} -\dfrac{\omega_{e1}\psi_f}{L_s} \\ -\dfrac{\omega_{e2}\psi_f}{L_s} \\ -\dfrac{\omega_{e3}\psi_f}{L_s} \\ -\dfrac{\omega_{e4}\psi_f}{L_s} \end{bmatrix}}_{\mathbf{z}(k)}
$$

$$
\underbrace{\begin{bmatrix} \sum F_{xj}(k) \\ M_z(k) \end{bmatrix}}_{\mathbf{y}(k)} = \underbrace{\begin{bmatrix} -\dfrac{p_n\psi_f\omega_{e1}L_s}{RR_{f1}} & \dfrac{dp_n\psi_f\omega_{e1}L_s}{2RR_{f1}} \\ \dfrac{p_n\psi_f}{R} & -\dfrac{dp_n\psi_f}{2R} \\ -\dfrac{p_n\psi_f\omega_{e2}L_s}{RR_{f2}} & -\dfrac{dp_n\psi_f\omega_{e2}L_s}{2RR_{f2}} \\ \dfrac{p_n\psi_f}{R} & \dfrac{dp_n\psi_f}{2R} \\ -\dfrac{p_n\psi_f\omega_{e3}L_s}{RR_{f3}} & \dfrac{dp_n\psi_f\omega_{e3}L_s}{2RR_{f3}} \\ \dfrac{p_n\psi_f}{R} & -\dfrac{dp_n\psi_f}{2R} \\ -\dfrac{p_n\psi_f\omega_{e4}L_s}{RR_{f4}} & -\dfrac{dp_n\psi_f\omega_{e4}L_s}{2RR_{f4}} \\ \dfrac{p_n\psi_f}{R} & \dfrac{dp_n\psi_f}{2R} \end{bmatrix}^T}_{\mathbf{C}} \underbrace{\begin{bmatrix} i_{d1}(k) \\ i_{q1}(k) \\ i_{d2}(k) \\ i_{q2}(k) \\ i_{d3}(k) \\ i_{q3}(k) \\ i_{d4}(k) \\ i_{q4}(k) \end{bmatrix}}_{\mathbf{x}(k)}
$$

$$
+ \underbrace{\begin{bmatrix} -\dfrac{p_n\psi_f^2}{R}\left(\dfrac{\omega_{e1}}{R_{f1}} + \dfrac{\omega_{e2}}{R_{f2}} + \dfrac{\omega_{e3}}{R_{f3}} + \dfrac{\omega_{e4}}{R_{f4}}\right) \\ -\dfrac{dp_n\psi_f^2}{2R}\left(-\dfrac{\omega_{e1}}{R_{f1}} + \dfrac{\omega_{e2}}{R_{f2}} - \dfrac{\omega_{e3}}{R_{f3}} + \dfrac{\omega_{e4}}{R_{f4}}\right) \end{bmatrix}}_{\mathbf{r}}. \quad (14)
$$

In the MPC framework, a cost function must be specified to find the optimal control sequences. The objectives can be achieved by minimizing the cost function

$$
\min_{u(k+h|k)} J = \sum_{h=1}^{H} [a\|\mathbf{y}(k+h\,|\,k) - \mathbf{y_{ref}}(k+h\,|\,k)\|^2 \\ + (1-a)(\mathbf{x}^T(k+h\,|\,k)\mathbf{u}(k+h-1\,|\,k))] \quad (15)
$$

where $(k+h|k)$ denotes the value predicted for time step $k+h$ based on the information available at time step k, and H is the prediction and control horizon. a is the tradeoff coefficient between the two optimization objectives.

In the cost function (15), the first penalty term reflects the tracking performance regarding the longitudinal forces and yaw moment, i.e., the desired planar motion performance. The output prediction $\mathbf{y}(k+h|k)$ can be computed recursively from the state-space model (14). The primary control objective of minimizing the total power consumption is achieved by minimizing the second penalty term in the cost function, which represents the total power consumption of four motors.

The control actions computed by the MPC-based scheme must satisfy the power-supply inverter output voltage constraints. Furthermore, considering the service life and safety of the PMSM, current limitations are also necessary. Taking these two facts into consideration, we impose the following linear inequality constraints

$$
\begin{aligned} -i_{d,max} &\le i_{dj}(k+h\,|\,k) \le i_{d,max} & h=1,2,...,H \\ -i_{q,max} &\le i_{qj}(k+h\,|\,k) \le i_{q,max} & h=1,2,...,H, \end{aligned} \quad (16)
$$

$$
\begin{aligned} -u_{d,max} &\le u_{dj}(k+h\,|\,k) \le u_{d,max} & h=1,2,...H \\ -u_{q,max} &\le u_{qj}(k+h\,|\,k) \le u_{q,max} & h=1,2,...H. \end{aligned} \quad (17)
$$

According to the motor model, the electromagnetic torque can be expressed as a function of the motor currents i_d and i_q. The currents are determined by the input voltages and electrical angular velocity of motors. Once the motor voltage and current constraints are determined, the torque constraint varies with the electrical angular velocity. By this means, there is no need to consider the constraints of the output torque, which can reduce the number of constraints to be processed.

As mentioned in section II-A, the planar motions with small wheel steering angles and medium speed and acceleration are studied in this paper. Therefore, the constraint of the road adhesion force is omitted. The prediction model (14), cost function (15) together with the constraints (16) and (17) constitute the MPC problem formulation of the MPC-based scheme. The problem can be formulated as a constrained quadratic programming problem which can be solved efficiently.

IV. SIMULATION STUDIES

A. Simulation Setup

In this section, several sets of simulations are conducted to validate the effectiveness of the MPC-based torque distribution scheme. All simulations are implemented in MATLAB/Simulink and CarSim co-simulation environments. The high-fidelity 4WID-EV model consisting of the vehicle dynamics model, driver model, and road information is developed in CarSim. The detailed parameters of the vehicle body of B-Class Hatchback in CarSim are listed in Table I. The reference model, four PMSMs, the vehicle dynamics controller, and the MPC-based scheme are developed in MATLAB/Simulink. While establishing the PMSM model, the equivalent iron loss resistance can be expressed as

$$
R_f = \frac{1}{K_e + K_h / n} \quad (18)
$$

where K_e and K_h are the eddy current loss and hysteresis loss coefficients of the PMSM respectively and n is the rotating speed according to [29],[30]. The detailed parameters of the PMSM are listed in TABLE II. The sampling period is set to T_s

= 1ms. The co-simulation diagram is shown in Fig.4.

In addition, in order to validate the effectiveness of the MPC-based scheme, a conventional control scheme without MPC is implemented as the benchmark. In the benchmark, the virtual torque distribution is computed by static quadratic programming approach and the torque on each wheel is achieved by the closed-loop field-oriented control.

TABLE I
MAIN VEHICLE MODEL PARAMETERS

Symbol	Description	Value
m	vehicle sprung mass	1110kg
L_f	the front semi wheelbase	1.04m
L_r	the rear semi wheelbase	1.56m
d	the width of the vehicle	1.48m
I_z	vehicle yaw moment of inertia	1343.1kg·m²
R	the tire effective radius	0.298m

TABLE II
PMSM PARAMETERS

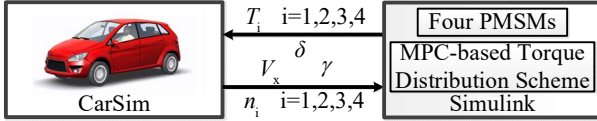| Symbol	Description	Value
L_d	d-axis inductance	6.43×10^{-4}H
L_q	q-axis inductance	6.43×10^{-4}H
R_s	armature resistance	0.096Ω
p_n	number of pole pairs	12
J	moment of inertia	0.201kg·m²
Ψ_f	magnet flux linkage	0.12747Wb
V	DC link voltage	300V
I	rated current	65.5A
P	rated power	5kW
K_e	eddy current loss coefficient	0.00682
K_h	hysteresis loss coefficient	6.05

Fig. 4. The co-simulation environment.

Two typical planar motion maneuvers are simulated in this study. The first maneuver contains a longitudinal acceleration, a single-lane change, and a longitudinal deceleration motion. A New European Driving Cycle (NEDC) is conducted as the second maneuver. Because of the manufacturing inconsistency and fatigue of electric circuits, the efficiencies of PMSMs could be varied [15]. Since this situation is widespread, we simulated the above two maneuvers in the case of different efficiency of motors on the front and rear axle. To imitate this difference, two power resistor packages were serially connected into the circuits of the rear two PMSMs, which makes the efficiencies of the front two motors higher than those of the rear two motors. The efficiency maps of the two kinds of motors are illustrated in Fig. 5. From the efficiency map, we can find that in the low rotational speed and large torque region, the motor efficiency is low especially in the regenerative braking situation. In the high rotational speed region, the motor efficiency always remains high. Therefore, it is necessary to optimize the energy efficiency of the 4WID-EV by reasonable torque distribution.

B. Acceleration, Single-Lane Change and Deceleration Maneuver

In this maneuver, the initial longitudinal velocity is 40km/h. First, the vehicle accelerates from 40km/h to 50km/h. Then, the vehicle turns with the peak wheel steering angle 2 rad followed by a deceleration motion in which the longitudinal velocity is
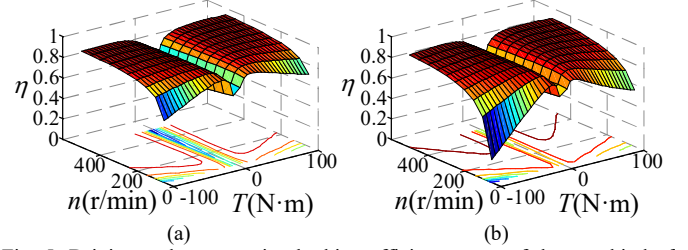
reduced from 50km/h to 40km/h.

Fig. 5. Driving and regenerative braking efficiency map of the two kind of PMSM. (a) Higher-efficiency motor. (b) Lower-efficiency motor.

As illustrated in Fig. 6, it can be seen intuitively that both schemes with and without MPC ensure excellent tracking performance of the desired longitudinal velocity and yaw rate. The square sum of the tracking errors of the longitudinal velocity and yaw rate listed in Table III indicates that the proposed MPC scheme has slightly better performances, of which the values are separately 0.8858, 4.1228×10^{-5} for benchmark and 0.8798, 3.1622×10^{-5} for the proposed MPC scheme. However, the torque distributions of the two schemes are quite different as illustrated in Fig. 7 (a) and (b). The torques computed by the scheme without MPC are always evenly distributed during the acceleration and deceleration motion. In the single lane change motion, the torques vary gradually with the vehicle turning and are evenly distributed between motors on the same side. Nevertheless, for the MPC-based scheme, the two high-efficiency motors always generate larger torques than the two low-efficiency motors during the whole maneuver due to the optimization of energy efficiency in the MPC algorithm. During the maneuver, the maximum driving torque of high-efficiency motors increased from 67.95N·m to 88.83N·m and the maximum regenerative breaking torque increased from 47.44N·m to 59.57N·m, while the torques of low-efficiency motors decrease from 67.95N·m and 47.44N·m to 45.4N·m and 33.56N·m respectively. The torque difference between the front and rear motors on the same side in the driving situation is larger than that in the regenerative braking situation of which the maximum is 43.43N·m and 26.01N·m due to the different efficiency characteristics of PMSMs in driving and braking conditions.
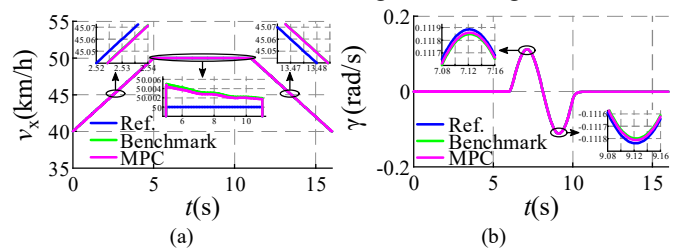

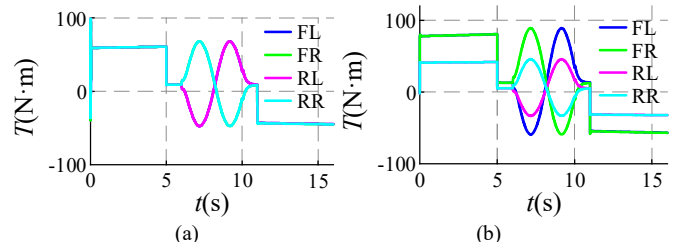Fig. 6. Tracking performance of the two schemes. (a) Longitudinal velocity. (b) Yaw rate.

Fig. 7. Torque distributions of the two schemes. (a) Benchmark. (b) MPC-based scheme.

The power consumption of the two schemes, reduction in power consumption of the MPC-based scheme compared with the benchmark and the related ratio are shown in Fig. 8 and Fig. 9. The proposed MPC-based scheme consumes significantly less power than the scheme without MPC during the whole maneuver. During the acceleration, the power reduction is more significant with a maximum value of 0.24kW. The ratio of power reduction to total power consumption reaches a maximum of 4.77% during the single lane change motion. The specific values of energy consumption and improved percentage are presented in TABLE III.

TABLE III
COMPARISON RESULTS OF DIFFERENT MANEUVERS

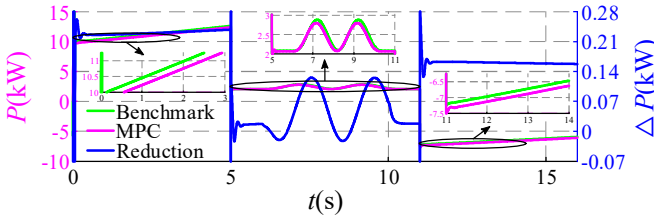| Maneuver | Energy consumption | | | Square sum of tracking errors | | | |
| | | | | Benchmark | | MPC-based scheme | |
	Benchmark	MPC-based scheme	Improved percentage	Longitudinal velocity	Yaw rate	Longitudinal velocity	Yaw rate
1st Maneuver	37.49kJ	35.29kJ	5.87%	0.8858	4.1228×10^{-5}	0.8798	3.1622×10^{-5}
2nd Maneuver	165.47kJ	159.07kJ	3.87%	2412.9	—	2396.4	—

Fig. 8. Power consumption of the two schemes and reduction in power consumption of the MPC-based scheme compared with benchmark.
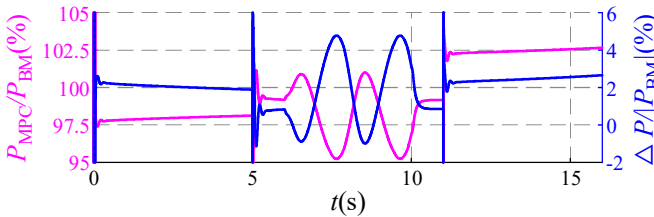

Fig. 9. Ratio of power reduction to the power consumption of the benchmark and ratio of power consumption of the two schemes.

The relationship between the vehicle speed and ratio of power loss to sum of four torques is illustrated in Fig. 10. The ratio in acceleration motion increases slightly as the vehicle speeds up, and similarly in deceleration motion, the ratio decreases slightly as the vehicle slows down from Fig. 10. This is because the iron loss is positive related to the motor rotational speed. During the whole maneuver, the magnitude of the ratio of the MPC scheme is smaller than that of the benchmark, which indicates that the proposed MPC scheme is effective in reducing the iron loss. Especially in the lane change motion, the performance is more obvious.
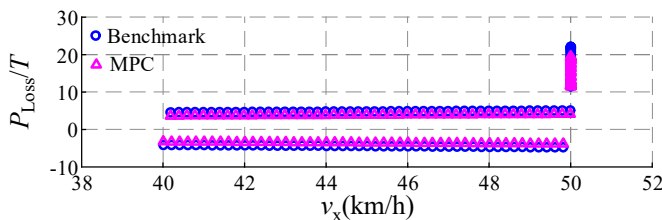

Fig. 10. Power loss versus sum of torques under different speeds.

C. NEDC Maneuver

NEDC was known as the most objective standard cycle for energy consumption and emission test [31]. In order to reduce the computational cost, the period from 0s to 195s, which can represent usual driving scenarios, is conducted to compare these two schemes.

The tracking performance of the longitudinal velocity is illustrated in Fig. 11. The longitudinal velocity with and without MPC both can follow the reference well. The square sum of tracking errors can be found in Table III of which the value is respectively 2412.9 for benchmark and 2396.4 for the MPC scheme indicating that the MPC scheme performs slight better than the benchmark. Since there is no steering in the NEDC maneuver, the tracking errors of yaw rate are omitted. The allocated torques of schemes with and without MPC are illustrated respectively in Fig. 12 (a) and (b). The torques of the scheme without MPC are always evenly distributed during the NEDC. However, in the MPC-based scheme, the front high-efficiency motors generate larger driving and regenerative braking torques than the rear low-efficiency motors, except that the torques reach the limit in some acceleration scenarios due to the limitation of voltages and currents. During the maneuver, the maximum driving torque of high-efficiency motors increased from 79.88N·m to 98.37N·m and the maximum regenerative breaking torque increased from 87.65N·m to 100N·m, while the torques of low-efficiency motors decrease from 79.88N·m and 87.65N·m to 61.39N·m and 73.51N·m respectively.

From Fig. 13 and Fig. 14, the power consumption of the MPC-based scheme is significantly lower than that of the scheme without MPC during the NEDC maneuver, except when the torques reach the limit. The maximum value of power
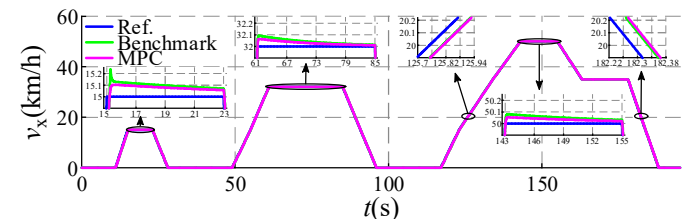

Fig. 11 Tracking performance of longitudinal velocity of two schemes during the NEDC.
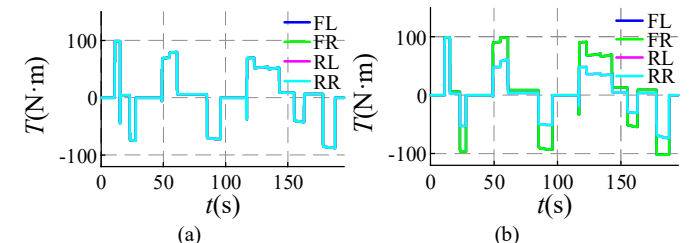

Fig. 12. Torque distributions of the two schemes. (a) Benchmark. (b) MPC-based scheme.

reduction is 0.14kW. The ratio of power reduction to total power consumption is larger during the acceleration and deceleration motion, indicating that the proposed MPC scheme is more effective in reducing power consumption in these scenarios. The total energy consumption of both schemes and improved percentage by the MPC-based scheme are listed in TABLE III.
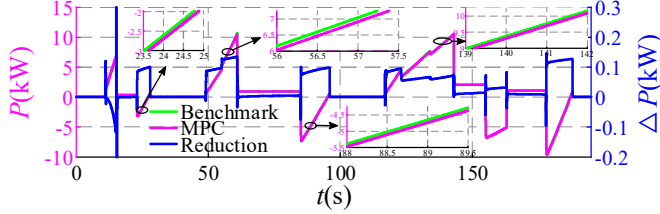

Fig. 13. Power consumption of the two schemes and reduction in power consumption of the MPC-based scheme compared with benchmark.
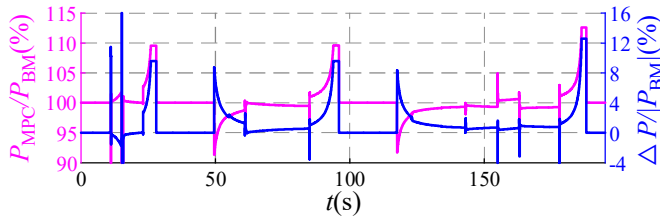

Fig. 14. Ratio of power reduction to the power consumption of the benchmark and ratio of power consumption of the two schemes.

To investigate the performance of the proposed MPC scheme in reducing iron loss in NEDC maneuver, we draw the Fig. 15 to illustrate the relationship between the speed and ratio of power loss to sum of four torques. From Fig. 15, whether during acceleration or deceleration, the higher the vehicle speed, the greater the ratio due to the positive correlation between vehicle speed and iron loss. Unlike the first maneuver, in the NEDC maneuver, there are several scenarios where the vehicle travels at a constant longitudinal velocity. Due to small torques, the proportion of iron loss in the motor power loss increases, especially in the case of high speed. From Fig.15, it can be concluded that the magnitude of the ratio of the MPC scheme is smaller than that of the benchmark when the vehicle travels at a constant speed, which indicates that the MPC scheme is effective in reducing the iron loss.
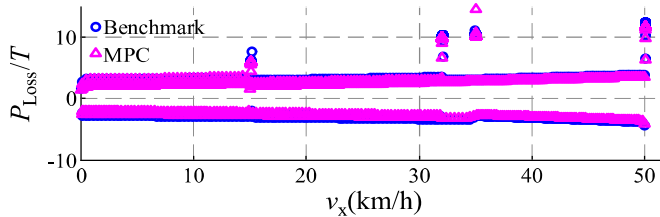

Fig. 15. Power loss versus sum of torques under different speeds.

D. Control effect and computation time

The performance of MPC relies on the length of prediction horizon to some extent. In general, the performance of MPC will be improved with a longer prediction horizon. However, longer prediction horizon increases the computational burden, which may make the MPC impractical for real-time applications. In this subsection, we investigate the tradeoff between computation time and control performance. Several sets of simulations of the two maneuvers are conducted for

different prediction horizon H from 1-time step to 10-time steps. Then the computation time and control performance are compared. Here the control performance is measured by total energy consumption. The results are illustrated in Fig. 16.

From Fig. 16, it's clear that the control performance is becoming better with the increase of the prediction horizon. When the prediction horizon length is longer than 6-time steps, the improvement of the control performance is no longer significant, but the average computation time spent in each control cycle has a striking increase. After trading off the computation time and control performance, the prediction horizon is selected as 6-time steps, and all the simulation results illustrated in section IV are with this prediction horizon length.
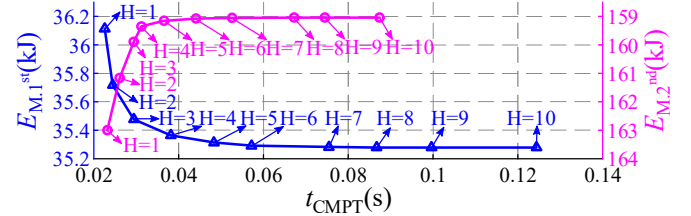

Fig. 16. Control performance versus average computation time for each control cycle.

V. CONCLUSION

This paper proposes an MPC-based torque distribution scheme for planar motions of 4WID-EVs to minimize the power consumption with guaranteed tracking performance. By incorporating the motor model considering iron losses in the MPC-based scheme design, the optimal torque distribution can be achieved without additional torque controllers by directly imposing the computed control signals to motors' terminals. The computational cost is lower because the constructed power consumption term to be optimized can be expressed as the product of the motor voltages and currents, which is simpler than that of the method using the efficiency map. After linearizing the motor model with reasonable assumptions, the control problem can be formulated as a constrained quadratic programming problem which can be solved efficiently. Several sets of simulations of two typical planar motion maneuvers are conducted. The results illustrate that the proposed MPC-based scheme consumes less power to accomplish excellent tracking of desired planar motions of 4WID-EVs.

REFERENCES

[1] Y. Hori, "Future vehicle driven by electricity and control——Research on four-wheel-motored 'UOT electric march II'," *IEEE Trans. Ind. Electron.*, vol. 51, no. 5, pp. 954-962, Oct. 2004.

[2] G. S. Buja and M. P. Lazmierkowski, "Direct torque control of PWM inverter-fed AC motors-a survey," *IEEE Trans. Ind. Electron.*, vol. 51, no.4, pp. 744-757, Aug. 2004.

[3] J. Kang, J. Yoo, and K. Yi, "Driving control algorithm for maneuverability, lateral stability, and rollover prevention of 4WD electric vehicles with independently driven front and rear wheels," *IEEE Trans. Veh. Technol.*, vol. 60, no. 7, pp. 2987-3001, Sep. 2011.

[4] Y. Chen and J. Wang, "Design and evaluation on electric differentials for over-actuated electric ground vehicles with four independent in-wheel motors," *IEEE Trans. Veh. Technol.*, vol. 61, no. 4, pp. 1534-1542, May 2012.

[5] M. Hua, G. Chen, B. Zhang, and Y. Huang, "A hierarchical energy efficiency optimization control strategy for distributed drive electric

vehicles," *Proc IMechE Part D: J. Automobile Engineering*, pp. 1-17, Nov. 2017.

[6] Pennycott, L. De Novellis, A. Sabbatini, P. Gruber, and A. Sorniotti, "Reducing the motor power losses of a four-wheel drive, fully electric vehicle via wheel torque allocation," *Proc Inst. Mech. Eng., Part D, J. Automobile Eng.*, vol. 228, no. 7, pp. 830-839, Jun. 2014.

[7] Z. Shuai, H. Zhang, J. Wang, J. Li, and M. Ouyang, "Lateral motion control for four-wheel-independent-drive electric vehicles using optimal torque allocation and dynamic message priority scheduling," *Control Eng. Practice*, vol. 24, pp. 55-66, 2014.

[8] J. Ni, J. Hu, and C. Xiang, "Envelope control of four-wheel independently actuated autonomous ground vehicle through AFS/DYC integrated control," *IEEE Trans. Veh. Technol.*, vol. 66, no. 11, pp. 9712-9726, Nov. 2017.

[9] X. Zhang, D. Göhlich, and J. Li, "Energy-efficient torque allocation design of traction and regenerative braking for distributed drive electric vehicles," *IEEE Trans. Veh. Technol.*, vol. 67, no. 1, pp. 285-295, Jan. 2018.

[10] Y. Chen and J. Wang, "Fast and global optimal energy-efficient control allocation with applications to over-actuated electric ground vehicles," *IEEE Trans. Control Syst. Technol.*, vol. 20, no. 5, pp. 1202-1211, Sep. 2012.

[11] S. Zhang, Y. Luo, J. Wang, X. Wang, and K. Li, "Predictive energy management strategy for fully electric vehicles based on preceding vehicle movement," *IEEE Trans. Intell. Transp. Syst.*, vol. 18, no. 11, pp. 3049-3060, Nov. 2017.

[12] R. Wang, Y. Chen, D. Feng, X. Huang, and J. Wang, "Development and performance characterization of an electric ground vehicle with independently actuated in-wheel motors," *J. Power Sources*, vol. 196, pp. 3962-3971, 2011.

[13] H. Zhou, F. Jia, H. Jing, Z. Liu, and L. Güvenç, "Coordinated longitudinal and lateral motion control for four-wheel independent motor-drive electric vehicle," *IEEE Trans. Veh. Technol.*, vol. 67, no. 5, pp. 3782-3790, May. 2018.

[14] D. Zhang, G. Liu, H. Zhou, and W. Zhao, "Adaptive sliding mode fault-tolerant coordination control for four-wheel independently driven electric vehicles," *IEEE Trans. Ind. Electron.*, vol. 65, no. 11, pp. 9090-9100, Nov. 2018.

[15] Y. Chen and J. Wang, "Adaptive energy-efficient control allocation for planar motion control of over-actuated electric ground vehicles," *IEEE Trans. Control Syst. Technol.*, vol.22, no. 4, pp. 1362-1373, Jul. 2014.

[16] M. Benosman, F. Lum, and J. L. Wang, "Nonlinear control allocation for non-minimum phase systems," *IEEE Trans. Control Syst. Technol.*, vol. 17, no. 2, pp. 394-404, Mar. 2009.

[17] J. Zheng, W. Su, and M. Fu, "Dual-stage actuator control design using a doubly coprime factorization approach," *IEEE Trans. Mechatronics*, vol. 15, no. 1, pp. 339-348, Jun. 2010.

[18] J. Wang and R. G. Longoria, "Coordinated and reconfigurable vehicle dynamics control," *IEEE Trans. Control Syst. Technol.*, vol. 17, no. 3, pp.723-732, May 2009.

[19] S. Chaithongsuk, B. Nahid-Mobarakeh, J. Caron, N. Takorabet, and F. Meibody-Tabar, "Optimal design of permanent magnet motors to improve field-weaking performances in variable speed drives," *IEEE Trans. Ind. Electron.*, vol. 59, no. 6, pp. 2484-2494, Jun. 2012.

[20] Z. Gmyrek, A. Boglietti, and A. Cavagnino, "Iron loss prediction with PWM supply using low- and high-frequency measurements: Analysis and results comparison," *IEEE Trans. Ind. Electron.*, vol. 55, no. 4, pp. 1722-1728, Apr. 2008.

[21] A. Watts, A. Vallance, A. Whitehead, C. Hilton, and A. Faster, "The technology and economics of in-wheel motors," *SAE Int. J. Passenger Cars-Electron. Electr. Syst.*, vol. 3, pp. 37-55, 2010.

[22] C. Mi, G. R. Slemon, R. Bonert, "Modeling of iron losses of permanent-magnet synchronous motors," *IEEE Trans. Ind. Appl.*, vol. 39, no. 3, pp. 734-742, 2003.

[23] J. Lee, K. Nam, S. Choi, and S. Kwon, "Loss-minimizing control of PMSM with the use of polynomial approximations," *IEEE Trans. Power Electron.*, vol. 24, no. 4, pp. 1071-1082, Apr. 2009.

[24] F. Fernndez-Bernal, A. Garcia-Cerrada, and R. Faure, "Determination of parameters in interior permanent magnet synchronous motors with iron losses without torque measurement," in Proc. *IEEE Ind. Appl. Conf.*, vol. 1, pp. 409-415, 2000.

[25] W. Deng, Y. Zhao, and J. Wu, "Energy efficiency improvement via bus voltage control of inverter for electric vehicles," *IEEE Trans. Veh. Technol.*, vol. 66, no. 2, pp. 1063-1073, Feb. 2017.

[26] S. Morimoto, Y. Tong, Y. Takeda, and T. Hirasa, "Loss minimization control of permanent magnet synchronous motor drives," *IEEE Trans. Ind. Electron.*, vol. 41, no. 5, pp. 511-517, Oct. 1994.

[27] K. Uezato, T. Senjyu, and Y. Tomori, "Modeling and vector control of synchronous reluctance motors including stator iron loss," *IEEE Trans. Ind. Appl.* Vol. 30, pp. 971-976, 1994.

[28] A. M. Dizqah and A. Sorniotti, "A fast and parametric torque distribution strategy for four-wheel-drive energy efficient electric vehicles," *IEEE Trans. Ind. Electron.*, vol. 63, no. 7, pp. 4367-4376, Nov. 2016.

[29] N. Urasaki, T. Senjyu, and K. Uezato, "An accurate modeling for permanent magnet synchronous motor drives," in *Appl. Power Electro. Conf.*, vol. 1, pp.387-392, 2000.

[30] Y. Li, J. Zhang, and K. Guo, "An accurate modeling for permanent magnet synchronous wheel motor including iron loss," *J. Alternative Powertrains*, vol. 3, no. 1, pp. 105-122, Jul. 2014.

[31] B. Zhu, D. Wu, M. Zheng, N. Zhang, and L. He, "Electric vehicle energy predictive optimal control by V2I communication," *Advances in Mechanical Engineering*, vol. 11, no. 2, pp. 1-16, Feb. 2019.

Yiyan Su was born in Qufu, Jining, Shandong, China in 1993. He received the B.S. degree in electrical engineering from University of Electronic Science and Technology of China, Chengdu, Sichuan, China, in 2016. He is currently pursuing the Ph.D. degree in electrical engineering at Xi'an Jiaotong University, Xi'an, Shaanxi, China.

His research interests include coordinated control of vehicles equipped with distributed drive systems, multi-time-scale hierarchical control strategy for complex multi-motor systems, power distribution and efficient control of hybrid energy storage systems and model predictive control.

Deliang Liang (Senior Member, IEEE) received the B.S., M.S. and Ph.D. degrees in Electrical Engineering from Xi'an Jiaotong University, Shaanxi, China in 1989, 1992 and 1996, respectively.
Since 1999, he has been with the School of Electrical Engineering, Xi'an Jiaotong University, where he is currently a professor. From 2001 to 2002, he was a visiting scholar with Science Solution International Lab., Tokyo, Japan. His research fields include optimal design, control, and simulation of electrical machines.

Peng Kou (Senior Member, IEEE) received his B.S. degree in electrical engineering from Xi'an Jiaotong University, China, in 2005. From the same university, he received his M.S. and Ph.D. degrees in control science and engineering in 2008 and 2013, respectively. From 2015 to 2016, he was a visiting scholar at The Ohio State University, Columbus, USA.

Currently he is a professor at the School of Electrical Engineering, Xi'an Jiaotong University. His research interests include model predictive control, motor control, and all electric aircraft.